THE JOURNAL OF PHYSICAL CHEMISTRY B

Article

pubs.acs.org/JPCB

Axial Ligand Effects on Vibrational Dynamics of Iron in Heme Carbonyl Studied by Nuclear Resonance Vibrational Spectroscopy

Takehiro Ohta,*[,†,▽] Jin-Gang Liu,[†,‡] Makina Saito,[§,∥] Yasuhiro Kobayashi,[§,¶] Yoshitaka Yoda,[#,¶] Makoto Seto,*[,§,⊥,¶] and Yoshinori Naruta*[,†,▽]

[†]Institute for Materials Chemistry and Engineering and International Institute for Carbon-Neutral Energy Research (WPI-I2CNER), Kyushu University, Fukuoka 812-8581, Japan

[▽]JST, ACT-C, Saitama 332-0012, Japan

[‡]Department of Chemistry, East China University of Science and Technology, 130 Meilong Rd, 200237, Shanghai, P. R. China

[§]Research Reactor Institute, Kyoto University, Osaka 590-0494, Japan

[⊥]Japan Atomic Energy Agency, Hyogo 679-5148, Japan

[#]Japan Synchrotron Radiation Research Institute, Hyogo 679-5198, Japan

[¶]CREST, Japan Science and Technology Agency, Saitama 332-0012, Japan

Supporting Information

ABSTRACT: Nuclear resonance vibrational spectroscopy (NRVS) and density functional theory calculation (DFT) have been applied to illuminate the effect of axial ligation on the vibrational dynamics of iron in heme carbonyl. The analyses of the NRVS data of five- (5c) and six-coordinate (6c) heme−CO complexes indicate that the prominent feature of ^{57}Fe partial vibrational density of state (^{57}FePVDOS) at the 250−300 cm^{-1} region is significantly affected by the association of the axial ligand. The DFT calculations predict that the prominent ^{57}FePVDOS is composed of iron in-plane motions which are coupled with porphyrin pyrrole in-plane (ν_{49}, ν_{50}, and ν_{53}), an out-of-plane (γ_8) (two of four pyrrole rings include the in-plane modes, while the rest of pyrrole rings vibrate along the out-of-plane coordinate), and out-of-phase carbonyl C and O atom displacement perpendicular to the Fe−C−O axis. Thus, in the case of the 5c CO−heme the prominent ^{57}FePVDOS shows sharp and intense feature because of the degeneracy of the *e* symmetry mode within the framework of C_{4v} symmetry molecule, whereas the association of the axial imidazole ligand in the 6c complex with the lowered symmetry results in split of the degenerate vibrational energy as indicated by broader and lower intensity features of the corresponding NRVS peak compared to the 5c structure. The vibrational energy of the iron in-plane motion in the 6c complex is higher than that in 5c, implying that the iron in the 6c complex includes stronger in-plane interaction with the porphyrin compared to 5c. The iron in-plane mode above 500 cm^{-1}, which is predominantly coupled with the out-of-phase carbonyl C and O atom motion perpendicular to Fe−C−O, called as Fe−C−O bending mode (δ_{Fe-C-O}), also suggests that the 6c structure involves a larger force constant for the *e* symmetry mode than 5c. The DFT calculations along with the NRVS data suggest that the stiffened iron in-plane motion in the 6c complex can be ascribed to diminished pseudo-Jahn−Teller instability along the *e* symmetry displacement due to an increased a_1−*e* orbital energy gap caused by σ^* interaction between the iron d_{z^2} orbital and the nitrogen p orbital from the axial imidazole ligand. Thus, the present study implicates a fundamental molecular mechanism of axial ligation of heme in association with a diatomic gas molecule, which is a key primary step toward versatile biological functions.

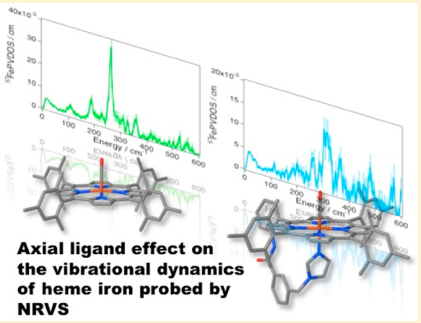

INTRODUCTION

Elucidation of the structure/function correlation of iron porphyrin is a pivotal issue in biological and materials chemistry, since a number of important material transformations involving O_2 activation are catalyzed at the active site of hemoproteins.[1] The cofactor heme involved in the enzyme is coordinated by an axial ligand from a protein side chain, which is a key structural motif to inspire the biological reactivity into the heme. The axial ligation of heme is crucial for the allosteric mechanism of hemoglobin for cooperative binding of O_2,[2] and would play a role in the ligand discrimination mechanism of hemoglobin and myoglobin[3] in conjunction with the role of heme distal environement.[4] Thus, extensive efforts have been devoted to address the fundamental mechanism of axial ligation of heme.[5−18]

The interactions between CO and hemoproteins have been extensively studied by spectroscopic methods to obtain fundamental insights into the molecular mechanism of binding

Received: May 7, 2012
Revised: September 12, 2012

 © XXXX American Chemical Society dx.doi.org/10.1021/jp304398g | J. Phys. Chem. B XXXX, XXX, XXX−XXX

of heme to diatomic gas molecules.[19−27] Heme−CO adducts are stable species, suitable for spectroscopic investigations. The advantage of high quantum yields for photodissociation of CO[20] allows studies of protein structural dynamics triggered by CO dissociation. The study of CO−heme interactions is crucial for elucidation of the signaling mechanism of CO sensor hemoproteins of CooA[28] and NPAS2.[29,30] CO is also known to activate soluble guanylate cyclase (sGC) in the presence of a cofactor, while the native mechanism of sGC is known to initiate signaling cascade with dissociating the axial ligand upon binding of NO for physiological functions.[16,31]

Resonance Raman (rR) spectroscopy provided valuable information on the vibrational properties of the axial coordination environment as well as the heme backbone structure to correlate the structural properties with the functions.[32−41] However, the rR spectroscopy involves the selection rule which hampers the observation of all vibrational modes of heme. Especially the assignments of low-frequency iron vibrational modes, the important determinant of the reactivity of heme,[42] are not facile. Thus, we exploited the nuclear resonance vibrational spectroscopy (NRVS)[43−46] to shed light on the effect of axial ligation on the vibrational dynamics of iron in a heme carbonyl complex. Since the first experiment[43a] and calculation of phonon density of state (PDOS),[43b] the synchrotron-based vibrational spectroscopy has emerged as a promising method to investigate the vibrational dynamics of biological iron without selection rules.[45] NRVS spectroscopy has been usefully applied to wide range of iron containing biological and inorganic complexes to characterize the coordination geometry and covalency with ligands, which is crucial for elucidation of biological reactions.[46] Heme carbonyl as a surrogate of an unstable diatomic ligand bound form such as heme−O_2 adduct is a useful species to perform spectroscopic analyses. Previously, Sage and co-workers carried out detailed NRVS and computational analyses of heme carbonyl species,[12] and characterized the important vibrational modes including iron in-plane motions, iron−axial imidazole stretching, and iron out-of-plane motions, which were difficult to observe with rR spectroscopy. The pioneering work of Sage and co-workers[12,45] encouraged us to investigate heme−carbonyl complexes using our functional model complex.[47] Previously, we have demonstrated that [Fe(TMP)Im] (where TMP is tetramesityl porphyrin, and Im is a tethered axial imidazole ligand) can transform a high-spin side-on peroxide to a low-spin end-on (hydro)peroxide intermediate, a key intermediate in biological dioxygen activation.[47] A side-on peroxy complex is considered as a dead-end species which is formed in the absence of axial ligation.[48] Thus, it is highly desirable to elucidate the molecular mechanism of axial ligation of heme at the atomic level using NRVS spectroscopy.

METHODS

Sample Preparation. $^{57}FeBr_2$ was prepared using a reference method.[49] $^{57}Fe_2O_3$ (>95%) was reacted with 47% aqueous HBr at 80 °C for 2 h to obtain $^{57}FeBr_3$. The ferric bromide in toluene was heated under Ar to yield $^{57}FeBr_2$. Preparations of [Fe^{III}(TMP)]Br and [Fe^{III}(TMP)Im]Br using $^{57}FeBr_2$ were performed by a published procedure.[47] [Fe^{III}(TMP)]Br and [Fe^{III}(TMP)Im]Br were reduced by sodium dithionite to yield the ferrous complexes in a glovebox. The 5c and 6c heme−CO complexes were prepared by a reported method:[15,50] bubbling of CO gas into 5 mM toluene solutions of [$^{57}Fe^{II}$(TMP)] and [$^{57}Fe^{II}$(TMP)Im][47] generated the corresponding heme−CO adducts.

NRVS Measurements and Analyses. For NRVS measurements, samples were loaded into thin Kapton taped 3.0 × 10.0 × 1.0 mm^3 cuvettes and frozen. ^{57}Fe NRVS spectra were recorded at BL09XU at SPring8[51a] using published procedures. During data collection the sample was maintained at low temperature using a liquid He cryostat (head temperature <10 K). Spectra were recorded between −20 and 80 meV in 0.25 meV steps, by detecting delayed nuclear resonance fluorescence and Fe K fluorescence (from internal conversion) with an APD array detector. The monochromator energy scales were calibrated using iron foil. The sample was placed in a monochromatic X-ray beam, whose energy was scanned through 14.4 keV ^{57}Fe resonance using a high-resolution monochromator with a full width at half-maximum of 8 cm^{-1}.[51b] The measurements of the heme−CO complexes were performed at 100−170 K. Temperatures were calculated from the ratio of anti-Stokes to Stokes intensity via $S(-E) = S(E)\exp(-E/kT)$. The calculation of ^{57}Fe PVDOS from the NRVS raw data were performed by a Fourier deconvolution method.[52]

DFT Calculations and Description of Normal Modes. All DFT calculations were carried out on the Gaussian 03 program[53] using Becker's three-parameter exchange and the Lee−Yang−Parr correlation (B3LYP)[54−56] functional. The basis set chosen for the heme−CO adducts is 2-fold: 6-311g*[57−59] for the Fe and CO atoms and 6-31g* for the rest of atoms. Our DFT calculation is composed of the geometry optimization of the heme−CO adducts and vibrational analyses of the fully converged structures. As pointed out previously,[45] it is crucial to perform DFT calculations on the complete model rather than on a truncated model system as experimental data showed that the porphyrin peripheral groups significantly influence the Fe vibrational dynamics. The information of the atomic displacements from the DFT calculations was used to calculate mode composition factors using eq 1, where $r_{j\alpha}$ is the displacements of the jth atom in the α mode and m_j is the mass of that atom.[45,60]

$$e_{j\alpha}{}^2 = \frac{m_j r_{j\alpha}{}^2}{\sum_j m_j r_{j\alpha}{}^2} \tag{1}$$

The NRVS intensity for a given normal mode is proportional to the motion of the resonance nucleus along the direction of the incident X-ray beam. For a randomly oriented sample, a NRVS transition for normal mode α contributes a fraction ϕ to the normalized excitation probability $S(\bar{\nu})$ that is directly proportional to the Fe mode composition factor $e_{j\alpha}{}^2$ and inversely proportional to $\bar{\nu}_\alpha$.[43b,60]

$$\phi_\alpha = \frac{1}{3}\frac{\bar{\nu}_R}{\bar{\nu}_\alpha} e_{j\alpha}{}^2 (\bar{n}_\alpha + 1) f \tag{2}$$

In the above equation, $\bar{\nu}_\alpha$ is the difference between the photon energy and the recoil-free nuclear resonance energy in wavenumbers, $h c\bar{\nu}_R = E_\gamma{}^2/2m_{Fe}c^2 = 1.96$ meV is the recoil energy of a free ^{57}Fe nucleus upon absorption of a photon energy $E_\gamma = 14.4$ keV, $\bar{n}_\alpha = [\exp(hc\bar{\nu}_\alpha/k_B T - 1]^{-1}$ is the thermal occupation factor for a mode of frequency at temperature T,[60] and the recoilless fraction $f = 1 - \sum\phi$. It is also useful to define an ^{57}Fe-centered partial vibrational density of states (PVDOS), $D_{Fe}(\bar{\nu})$, using a line-shape function $L((\bar{\nu} - \bar{\nu}_\alpha)$:[45b,60]

dx.doi.org/10.1021/jp304398g | J. Phys. Chem. B XXXX, XXX, XXX−XXX

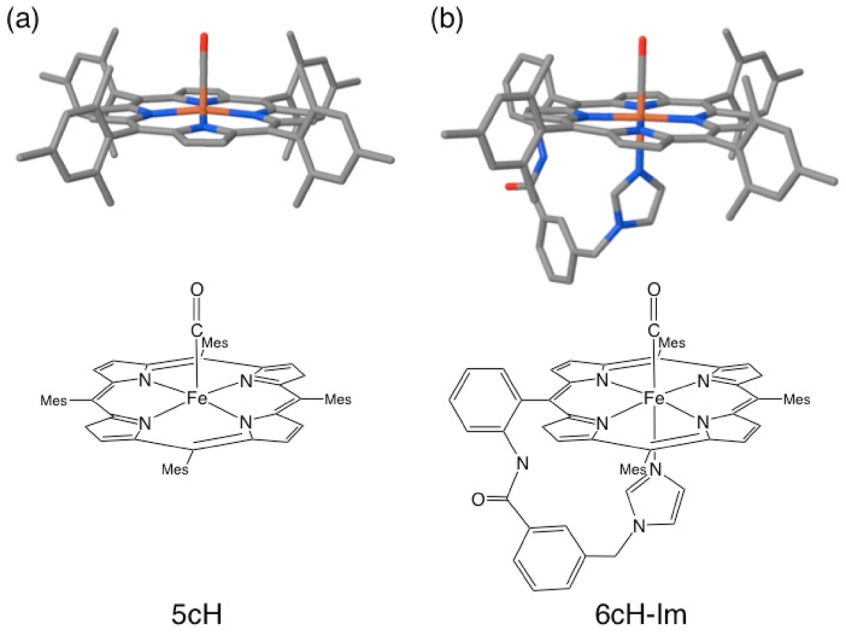

Figure 1. Structures of 5c (a) and 6c (b) heme carbonyl complexes, indicated as 5cH and 6cH−Im, respectively, where Mes indicates a mesityl group.

$$D_{Fe}(\bar{\nu}) = \sum_{\alpha} e^2_{Fe,\alpha} L(\bar{\nu} - \bar{\nu}_{\alpha}) \quad (3)$$

The calculation of the mode composition factor and the simulation of NRVS spectra were performed by the Gennrvs program.[61]

RESULTS

Structures of Heme−CO Adducts. The DFT-optimized structures of the 5c and 6c heme−CO complexes are shown in Figure 1, and the selected geometrical parameters are listed in Table 1. X-ray crystal structural analyses of heme−carbonyl complexes have shown that the Fe−CO distance of 6c CO−heme adducts appears in the range of 1.74−1.79 Å depending on the porphyrin substituent and axial ligand,[62] while the 5c adducts include shorter Fe−CO distances of ∼1.71 Å.[63] The present DFT calculations show fairly good agreement with the crystal structural data. The C−O distance, on the other hand, is insensitive to the axial ligation, indicating that iron d_π back-donation into the CO π^* orbital is not affected by the σ-donation from the axial imidazole ligand.[63] The equatorial Fe−N_{por} bond lengths of the 5c and 6c structures are also almost the same values, indicative of a little influence of the axial coordination on the Fe−N_{por} π bonding. The Fe−Im bond distance of 2.08 Å in the 6c complex is also reasonable from the X-ray crystal structures,[62] and the projection of the imidazole plane onto the porphyrin lies along the bisection of one of the N_{por}−Fe−N_{por} angles. Our model includes the tethered imidazole axial ligand attached to the phenyl substituent, which would give different vibrational aspects compared to the previously studied more symmetrical tetraphenyl substituted porphyrin,[12] due to the lowered symmetry in our model complex.

Table 1. Selected Optimized Geometrical Parameters of Heme−CO Adducts[a]

	5cH	6cH−Im
Fe−C	1.73	1.79
C−O	1.15	1.14
Fe−N_{Por}[b]	2.01	2.02
Fe−N_{Im}	–	2.08

[a]The unit in angstroms. [b]The averaged distances.

Scheme 1. Schematic Drawing of Selected Vibrational Modes in 5cH

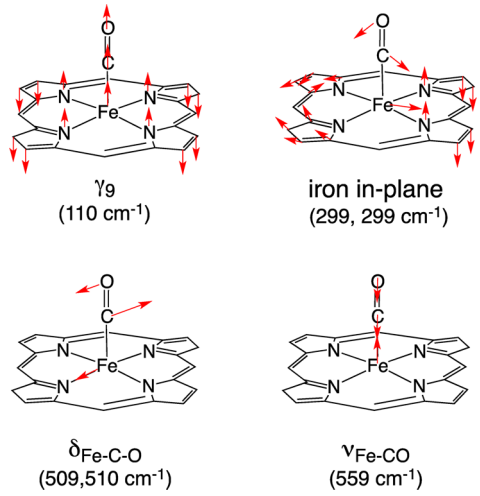

NRVS Analyses. *5c Heme−CO Adduct.*[64] The ^{57}FePVDOS derived from the NRVS data of 5c heme−CO complex and the predicted ^{57}FePVDOS obtained by the DFT calculation are shown in Figure 2. The experimental data shown by the green line with error bar is overlaid with the green filled Gaussian functions obtained by the DFT-based normal-coordinate analysis. All frequencies are unscaled output from the DFT calculation.

While the vibrational energy of the prominent ^{57}FePVDOS peak calculated by the DFT calculation is somewhat higher than that of the experimental data, there is good agreement

dx.doi.org/10.1021/jp304398g | J. Phys. Chem. B XXXX, XXX, XXX−XXX

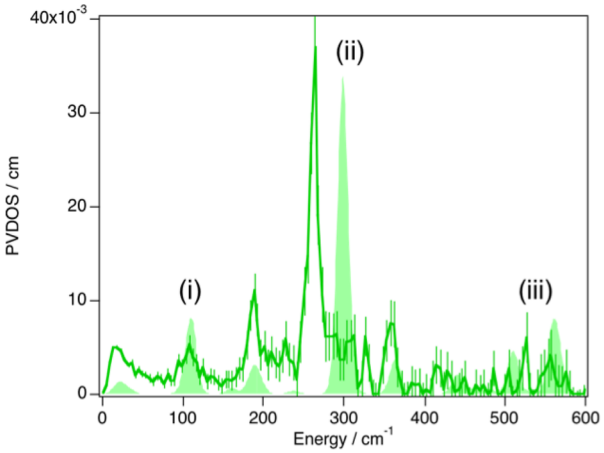

Figure 2. Comparison between the measured (green solid line with error bars) and predicted (green filled Gaussian functions) ^{57}FePVDOS for the 5c heme−CO adduct; the γ_9 (i), iron in-plane (ii), and Fe−CO stretching and Fe−C−O bending modes (iii).

between the experimental and the predicted data regarding the relative intensities of the NRVS peaks without frequency scaling.[65] According to the previous NRVS studies by Rai et al. and Leu et al. on a 6c heme carbonyl complex,[12] modes above 500 cm^{-1} are associated with the FeCO group, in-plane vibrations dominate the 300−400 cm^{-1} region, and Fe motion is predominantly out of plane for modes with frequencies below 220 cm^{-1}.

From our DFT-based ^{57}FePVDOS simulation, the most intense feature of the experimental ^{57}FePVDOS around 260 cm^{-1} would be assigned as iron in-plane motions coupled with out-of-phase carbonyl C and O atom displacements perpendicular to the Fe−C−O axis, porphyrin in-plane ν_{49}, ν_{50}, and ν_{53},[25−32] and out-of-plane γ_8 modes:[36] two of four pyrrole rings include the mixed in-plane vibrational modes, while the rest of the pyrrole shows the out-of-plane motion. The degenerate iron in-plane *e* symmetry motion due to the C_{4v} symmetry of the molecule is represented by sharp and intense features of the prominent ^{57}FePVDOS peak. The iron in-plane displacement is not directed to the nitrogen atom of porphyrin pyrroles, but a motion of bisect along the one of the N_{por}−Fe−N_{por} angles.

The relative ratio of the peak intensity from the prominent iron in-plane motion and the peaks associated with Fe−CO modes is about 5, which is nearly twice that of 6c CO−heme adducts.[12] Thus, in the 5c complex, the in-plane motion is larger than in the 6c complex due to a softened iron in-plane force constant as will be discussed below.

The DFT calculation characterized the Fe−CO stretching (ν_{Fe-CO}) and the iron in-plane mode coupled mostly with the out-of-phase C and O atom displacements perpendicular to the Fe−C−O axis, called as Fe−C−O bending (δ_{Fe-C-O}) modes, at 559[67] and 510 cm^{-1}, respectively, whereas the NRVS spectrum shows the plausible corresponding peaks at 550 and 520 cm^{-1}, respectively. This is a reverse trend compared to 6c iron−carbonyl species that include the ν_{Fe-CO} modes at lower frequencies (470−510 cm^{-1}) than the δ_{Fe-C-O} modes (550−570 cm^{-1}),[15,18,19,50] indicating that the axial ligation strengthens the Fe−C−O bending force constant with lowering the Fe−CO bond strength.

The NRVS feature observed at 110 cm^{-1} can be assigned as the doming mode (γ_9) that exhibits iron out-of-plane displacement while the periphery of the porphyrin moves in the opposite direction[12,67] as the DFT predicted the mode at the same position. This out-of-plane iron motion is considered as an important determinant of the reactivity of heme toward diatomic gas molecules.[42,67]

6c Heme−CO Adduct. The ^{57}FePVDOS derived from the NRVS data of the 6c heme−CO complex and the simulation at the B3LYP DFT theory level are shown in Figure 3. The

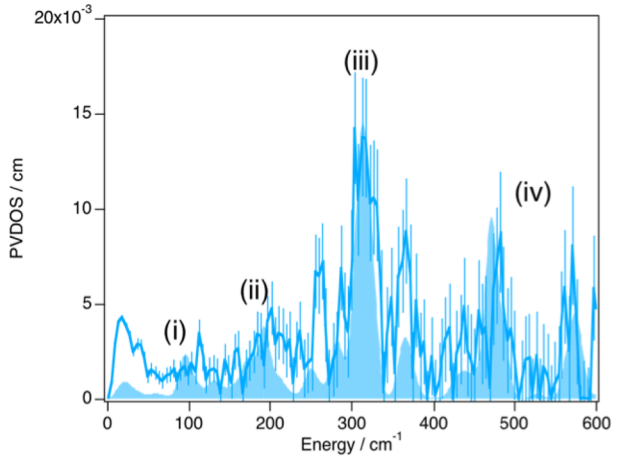

Figure 3. Comparison between the measured (aqua solid line with error bars) and predicted (aqua filled Gaussian functions) ^{57}FePVDOS for the 6c heme−CO adduct; the γ_9 (i), Fe−Im stretching and bending (ii), iron in-plane (iii), and Fe−CO stretching and Fe−C−O bending modes (iv).

experimental ^{57}FePVDOS is shown by the aqua line with error bar, while the simulated data is represented with the aqua filled Gaussian functions. All frequencies are unscaled output from the DFT calculation.

The DFT-predicted ^{57}FePVDOS shows good agreement with the experimental data. The prominent features of ^{57}FePVDOS at ∼315 cm^{-1} can be assigned as the iron in-plane motion which is coupled with the out-of-phase motion of the CO moiety, porphyrin in-plane ν_{49}, ν_{50}, and ν_{53}, and out-of-plane γ_8 modes, as described for the 5c CO−heme complex. The DFT calculation indicates that the degenerate *e* symmetry iron in-plane motions appear at 308 and 317 cm^{-1}. The degeneracy is lifted one along imidazole plane (308 cm^{-1}) and the other perpendicular to the plane (317 cm^{-1}) with bisecting one of the N_{por}−Fe−N_{por} angles. The splitting of the energy for the iron in-plane motions is not large as observed for [Fe(TPP)(1-MeIm)(CO)],[12b] where the *x*−*y* splitting is ∼18 cm^{-1}, which can be ascribed to the lowered symmetry in our model complex. These vibrational energies of the 6c complex are higher than those of the 5c structure despite the Fe−N_{por} bond distances being almost the same for both species from the DFT calculations. The molecular mechanism of the stiffened *e* symmetry iron in-plane displacement in the 6c structure will be discussed in the following section.

The150−200 cm^{-1} region would be contributed predominantly by iron−imidazole (Fe−Im) bond, according to the previous report.[12b] The ^{57}FePVDOS features observed at 180−190 cm^{-1} would be associated with vibrational motion of the Fe−Im moiety, because the DFT calculation predicts the Fe−Im stretching (ν_{Fe-Im}) and bending (δ_{Fe-Im}) mode at 173 and 163 cm^{-1}, respectively, as shown in Scheme 2.[69] The mode composition factor (MCF) of selected atoms plotted in Figure 4 also supports the assignment of the vibrational mode,

dx.doi.org/10.1021/jp304398g | J. Phys. Chem. B XXXX, XXX, XXX−XXX

Scheme 2. Schematic Drawing of Fe−Im Vibrationas Modes in 6cH−Im

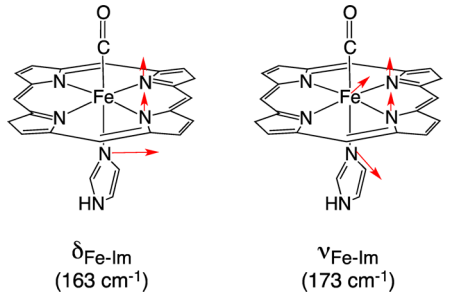

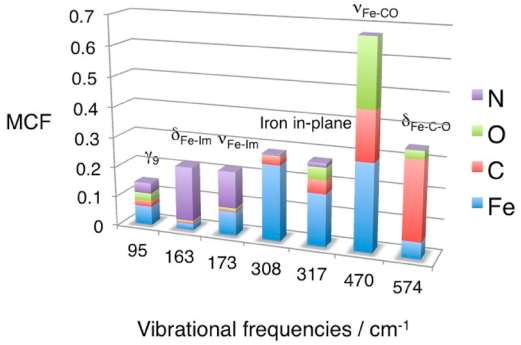

Figure 4. Plot of mode composition factors for the selected vibrational modes. The contributions from selected atoms are indicated by blue (Fe), red (carbon atom of CO), green (oxygen atom of CO), and purple (nitrogen atom of axial imidazole) blocks.

showing large kinetic energy contributions from the nitrogen atom of the axial imidazole ligand coordinating to the iron. This ν_{Fe-Im} mode frequency at 173 cm^{-1} is lower than the reported frequencies observed for the five-coordinate high-spin ferrous porphyrin,[6,7] suggesting that the σ-donation from the trans CO ligand weakens the Fe−Im bond in the 6c structure.

The ν_{Fe-CO} and δ_{Fe-C-O} modes characterized at 470[70] and 570 cm^{-1} are typical frequencies observed for other 6c heme carbonyl species using rR spectroscopy.[15,19,50] The δ_{Fe-C-O} is coupled with iron in-plane motions bisecting one of the N_{por}−Fe−N_{por} angles, while in the 5c structure the motion is along the N_{por}−Fe−N_{por} axis. Thus, the conformation of the axial ligand can alter the direction of the displacement of the C and O atom of the carbonyl.

The band at ∼110 cm^{-1} can be assigned as one of the doming mode (γ_9) of the complex,[68] because DFT predicts the corresponding mode at 94 cm^{-1}. Previously, the γ_9 mode was reported at 69 cm^{-1} for [Fe(TPP)(CO)(1-MeIm)] from refined normal-coordinate analyses to the NRVS data[12a] and at 94 cm^{-1} from DFT-based NCA analysis.[12b] From the NRVS analyses of the oriented sample, 39, 64, and 127 cm^{-1} modes were contributed by iron out-of-plane displacement, and 64 and 127 cm^{-1} modes were proposed to be associated with doming motions.[12b] The deviation of DFT-based NCA was ascribed to the computational model performed on an isolated molecule, in which translational and rotational motions do not interfere.[12b]

The appearances of the doming mode at ∼110 cm^{-1} for both 5c and 6c CO heme complexes are somewhat unexpected, because 6c CO heme might show a lower vibrational energy for the out-of-plane mode due to a mode coupling with an axial ligand. However, the present result suggests that the mode coupling in the 6c complex of our model is a minor effect, and rather coupling with the porphyrin peripheral substituent has dominant effect on the vibrational energy. The relative insensitivity of axial ligation to the doming mode was also pointed out by Leu et al.[12b] Our direct comparison between the 5c and 6c CO−heme adducts further supports the mechanism of doming vibration.

MO Analysis. The molecular orbital (MO) diagrams of the 5c and 6c CO−heme complexes are described to obtain insights into the correlation between the electronic and vibrational structures (Figure 5). Previously, the electronic

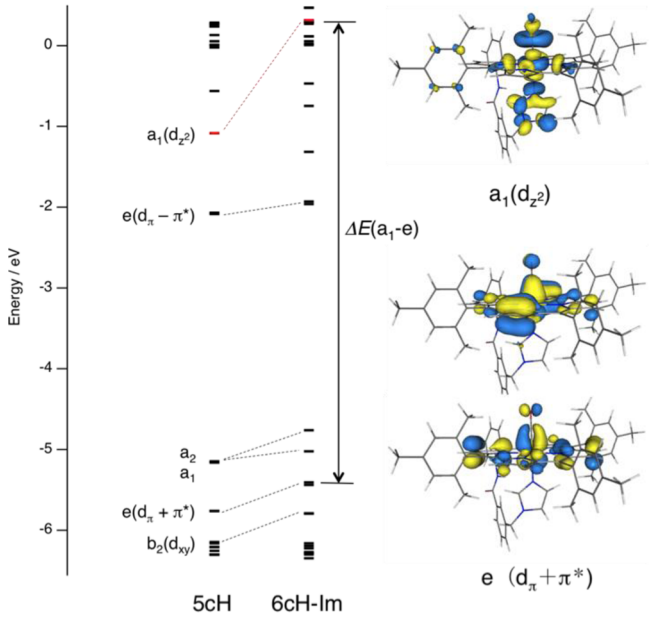

Figure 5. Molecular orbital diagram of heme−CO adducts.

structures of the 5c and 6c heme−CO adducts with different axial donor strengths were discussed by one of the authors using DFT calculations.[18] The large differences were observed at the energy level of an a_1 orbital that was composed of the d_{z^2} orbital of iron and σ^* orbital of CO, which is reproduced in this study using the larger model. This MO diagram would explain why the force constants of the e symmetry iron in-plane motions are stronger in the 6c than in the 5c complex with utilizing the pseudo-Jahn−Teller (pJT) theory.[71] According to the vibronic interaction theory, the mixing of a_1 and e electronic states, the direct product of which involves e symmetry vibration, can decrease the curvature of the adiabatic potential in the direction of the e displacements. The efficiency of the a_1 and e mixing is critically dependent on the energy gap (Δ) between the a_1 and e orbitals in the case of the singlet ground state.[18,71] Thus, in the 6c complex where the a_1−e energy gap is larger than that of the 5c complex is expected to show the stiffened e symmetry iron in-plane motions with reduced pJT instability for a Fe−C−O bent form.

DISCUSSION

The present NRVS and DFT analyses delineate the difference in the vibrational dynamics of iron in a heme carbonyl caused by the association of axial ligand. The large deviation can be observed in the prominent NRVS peak at 250−300 cm^{-1} region contributed by iron in-plane motions coupled with porphyrin in-plane and out-of-plane vibrations and the out-of-phase displacement of the carbonyl moiety. The vibrational

dx.doi.org/10.1021/jp304398g | J. Phys. Chem. B XXXX, XXX, XXX−XXX

energies of the iron in-plane mode and the δ_{Fe-C-O} mode are increased by the association with the axial ligation, which can be ascribed to a reduced pJT instability to a Fe−C−O bent structure derived from an increased a_1-e orbital energy gap through the σ^* interaction between the Fe d_{z^2} and nitrogen p orbital from the axial ligand.

The increased stability of the 6c CO−heme adduct with the Fe−C−O upright structure might be useful in the ligand discrimination mechanism of hemoglobin and myoglobin, where a distal histidine residue is placed above the heme iron, preventing the binding of CO to iron in a linear fashion. On the basis of quantum chemical calculations, Jewsbury and Kitagawa et al. previously pointed out that the proximal histidine residue is largely responsible for discouraging the binding of CO to the protein active site.[3] The present study also suggests the large influence of the imidazole axial ligation on the ligand discrimination mechanism of the oxygen carrier hemoproteins.

The decreased pJT instability in the axial ligand-associated model might have relevance with an efficient protonation of the side-on peroxy adduct formed in the presence of a tethered axial imidazole ligand.[47] Although the original side-on peroxy heme complex reported by Valentine and co-workers[48] was unable to protonate to generate a hydroperoxy complex, we have recently demonstrated that a side-on peroxy heme adduct containing the tethered axial imidazole ligand can be protonated efficiently with altering the peroxide binding mode from the side-on to end-on to accept the proton. Thus, the inability of protonation of the side-on peroxy adduct without any axial ligand might be ascribed to the pJT instability for the stable bent adduct, whereas the instability is removed in the presence of the axial ligand, allowing the formation of the protonated adduct with the end-on form. In other words, the formation of the dead-end side-on peroxo complex can be avoided with harnessing the axial ligand. Because a 6c low-spin hydroperoxy species is considered as a key intermediate for O−O bond cleavage,[47] the elucidation of the formation mechanism of this species is of profound importance in the O_2 activation chemistry.[72]

In summary, the present study delineates the effect of axial ligation on the vibrational dynamics of iron in heme carbonyl using the advantage of the relatively simple electronic and vibrational structures of the functional model complex, implicating a fundamental mechanism of the axial ligation of heme in association with a diatomic gas molecule, which is a key primary step toward the biological functions.

■ ASSOCIATED CONTENT

Ⓢ Supporting Information

DFT analysis of a bis CO bound porphyrin complex $[Fe(TMP)(CO)_2]$; simulation of the NRVS spectrum of $[Fe(TMP)(CO)_2]$; and a list of references used. This material is available free of charge via the Internet at http://pubs.acs.org.

■ AUTHOR INFORMATION

Corresponding Author

*E-mail: takehiro@ms.ifoc.kyushu-u.ac.jp (T.O.); seto@rri.kyoto-u.ac.jp (M.S.); naruta@ms.ifoc.kyushu-u.ac.jp (Y.N.).

Present Address

‖Sincrotrone Trieste in Area Science Park S.S., 14 Km 163, 5 34012 Basovizza (TS), Italy.

Notes

The authors declare no competing financial interest.

■ ACKNOWLEDGMENTS

This work was financially supported by Grants-in-Aid for Young Scientists (B) (no. 21750064, T.O.) from JSPS, MEXT project of Integrated Research on Chmiecal Synthesis to T.O. and Y.N., Innovative Areas (no. 20200050, J.G.L. and T.O.) from MEXT, and by the Elemental Science and Technology Project from MEXT to Y.N. The computations were partly carried out with help from the Research Institute for Information Technology, Kyushu University. The synchrotron radiation experiments were performed at the BL09XU of SPring-8 with the approval of the Japan Synchrotron Radiation Research Institute (JASRI) (Proposal No. 2009A1450 and 2010B1521). T.O. thanks Lei Liu (Stanford University) for his help of the setup of the Gennrvs program.

■ REFERENCES

(1) Sono, M.; Roach, M. P.; Coulter, E. D.; Dawson, J. H. *Chem. Rev.* **1996**, *96*, 2841−2887.

(2) Perutz, M. F. *Nature* **1970**, *228*, 726−739.

(3) (a) Jewsbury, P.; Yamamoto, S.; Minato, T.; Saito, M.; Kitagawa, T. *J. Am. Chem. Soc.* **1994**, *116*, 11586−11587. (b) Jewsbury, P.; Yamamoto, S.; Minato, T.; Saito, M.; Kitagawa, T. *J. Phys. Chem.* **1995**, *99*, 12677−12685.

(4) Spiro, T. G.; Kozlowski, P. M. *Acc. Chem. Res.* **2001**, *34*, 137−144 and references therein..

(5) Kitagawa, T. In *Biological Applications of Raman Spectroscopy*; Spiro, T. G., Ed.; Wiley-Interscience: New York, 1988; Vol. *3*, pp 97−130.

(6) Kitagawa, T.; Nagai, K.; Tsubaki, M. *FEBS Lett.* **1979**, *104*, 376−378.

(7) (a) Ohta, T.; Kitagawa, T. *Inorg. Chem.* **2005**, *44*, 758−769. (b) Uchida, T.; Kitagawa, T. *Acc. Chem. Res.* **2005**, *38*, 662−670 and references therein..

(8) Ghosh, A.; Bocian, D. F. *J. Phys. Chem.* **1996**, *100*, 6363−6367.

(9) Rovira, C.; Kunc, K.; Hutter, J.; Ballone, P.; Parrinello, M. *J. Phys. Chem. A* **1997**, *101*, 8914−8925.

(10) Smith, D. M. A.; Dupuis, M.; Vorpagel, E. R.; Straatsma, T. P. *J. Am. Chem. Soc.* **2003**, *125*, 2711−2712.

(11) Ohta., T.; Matsuura, K.; Yoshizawa, K.; Morishima, I. *J. Inorg. Biochem.* **2000**, *82*, 141−152.

(12) (a) Rai, B. K.; Durbin, S. M.; Prohofsky, E. W.; Sage, T. J.; Ellison, M. K.; Roth, A.; Scheidt, W. R.; Sturhahn, W.; Alp, E. E. *J. Am. Chem. Soc.* **2003**, *125*, 6927−6936. (b) Leu, B. M.; Silvernail, N. J.; Zgierski, M. Z.; Wyllie, G. R. A.; Ellison, M. K.; Scheidt, W. R.; Zhao, J.; Sturhahn, W.; Alp, E. E.; Sage, T. *Biophys. J.* **2007**, *92*, 3764−3783.

(13) Champion, P. M.; Stallard, B. R.; Wagner, G. C.; Gunsalus, I. C. *J. Am. Chem. Soc.* **1982**, *104*, 5469−5472.

(14) Xu, C.; Ibrahim, M.; Spiro, T. G. *Biochemistry* **2008**, *47*, 2379−2387.

(15) Vogel, K. M.; Kozlowski, P. M.; Zgierski, M. Z.; Spiro, T. G. *Inorg. Chim. Acta* **2000**, *297*, 11−17.

(16) Pal, B.; Li, Z.; Ohta, T.; Takenaka, S.; Tsuyama, S.; Kitagawa, T. *J. Inorg. Biochem.* **2004**, *98*, 824−832.

(17) Ohta, T.; Pinakoulaki, E.; Soulimane, T.; Kitagawa, T.; Varotsis, C. *J. Phys. Chem. B* **2004**, *108*, 5489−5491.

(18) Ohta, T.; Pal, B.; Kitagawa, T. *J. Phys. Chem. B* **2005**, *109*, 21110−21117.

(19) Spiro, T. G.; Wasbotten, I. H. *J. Inorg. Biochem.* **2005**, *99*, 34−44.

(20) Ye, X.; Demidov, A.; Champion, P. M. *J. Am. Chem. Soc.* **2002**, *124*, 5914−5924.

(21) Lim, M.; Jackson, T. A.; Anfinrud, P. A. *Science* **1995**, *269*, 962−966.

(22) Sage, J. T.; Schomacker, K. T.; Champion, P. M. *J. Phys. Chem.* **1995**, *99*, 3394−3405.
(23) Mizutani, Y.; Kitagawa, T. *Science* **1997**, *278*, 443−446.
(24) Bourgeois, D.; Vallone, B.; Schotte, F.; Arcovito, A.; Miele, A. E.; Sciara, G.; Wulff, M.; Anfinrud, P.; Brunori, M. *Proc. Natl. Acad. Sci. U.S.A.* **2003**, *100*, 8704−8709.
(25) Srajer, V.; Reinish, L.; Champion, P. M. *Biochemistry* **1991**, *30*, 4886−4895.
(26) Sato, A.; Gao, Y.; Kitagawa, T.; Mizutani, Y. *Proc. Natl. Acad. Sci. U.S.A.* **2007**, *104*, 9627−9632.
(27) Koutsoupakis, C.; Soulimane, T.; Varotsis, C. *J. Am. Chem. Soc.* **2003**, *125*, 14728−14732.
(28) Aono, S. *Acc. Chem. Res.* **2003**, *36*, 825−831.
(29) Dioum, E. M.; Rutter, J.; Tuckerman, J. R.; Gonzalez, G.; Gilles-Gonzalez, M. A.; McKnight, S. L. *Science* **2002**, *298*, 2385−2387.
(30) Boehning, D.; Snyder, S. H. *Science* **2002**, *298*, 2339−2340.
(31) (a) Friebe, A.; Schultz, G.; Koesling, D. *EMBO J.* **1996**, *15*, 6863−6868. (b) Ballou, D. P.; Zhao, Y.; Brandish, P. E.; Marletta, M. A. *Proc. Natl. Acad. Sci. U.S.A.* **2002**, *99*, 12097−12101 and references therein..
(32) Spiro, T. G. Resonance Raman Spectra of Heme and Metalloproteins In *Biological Applications of Raman Spectroscopy*; Wiley-Interscience: New York, 1988; Vol. 3.
(33) Kitagawa, T.; Abe, M.; Ogoshi, H. *J. Chem. Phys.* **1978**, *69*, 4516−4526.
(34) Abe, M.; Kitagawa, T.; Kyogoku, Y. *J. Chem. Phys.* **1979**, *69*, 4526−4534.
(35) (a) Li, X.-Y.; Czernuszewicz, R. S.; Kincaid, J. R.; Su, Y. O.; Spiro, T. G. *J. Phys. Chem.* **1990**, *94*, 31−47. (b) Li, X.-Y.; Czernuszewicz, R. S.; Kincaid, J. R.; Stein, P.; Spiro, T. G. *J. Phys. Chem.* **1990**, *94*, 47−61.
(36) Kozlowski, P. M.; Spiro, T. G.; Bérces, A.; Zgierski, M. Z. *J. Phys. Chem. B* **1998**, *102*, 2603−2608.
(37) Hu, S.; Morris, I. K.; Singh, J. P.; Smith, K. M.; Spiro, T. G. *J. Am. Chem. Soc.* **1993**, *115*, 12446−12458.
(38) Hu, S.; Smith, K. M.; Spiro, T. G. *J. Am. Chem. Soc.* **1996**, *118*, 12638−12646.
(39) Soldatova, A. V.; Ibrahim, M.; Olson, J. S.; Czernuszewicz, R. S.; Spiro, T. G. *J. Am. Chem. Soc.* **2010**, *132*, 4614−4625.
(40) Zeng, W.; Silvernail, N. J.; Wharton, D. C.; Georgiev, G. Y.; Leu, B. M.; Scheidt, W. R.; Zhao, J.; Sturhahn, W.; Alp, E. E.; Sage, J. T. *J. Am. Chem. Soc.* **2005**, *127*, 11200−11201.
(41) Adams, K. K.; Tsoi, S.; Yan, J.; Durbin, S. M.; Ramdas, A. K.; Cramer, W. A.; Sturhahn, W.; Alp, E. E.; Schulz, C. *J. Phys. Chem. B* **2006**, *110*, 530−536.
(42) Zhu, L.; Sage, J. T.; Champion, P. M. *Science* **1994**, *266*, 629−632.
(43) (a) Seto, M.; Yoda, Y.; Kikuta, S.; Zhang, X. W.; Ando, M. *Phys. Rev. Lett.* **1995**, *74*, 3828−3831. (b) Sturhahan, W.; Toellner, T. S.; Alp, E. E.; Zhang, X.; Ando, M.; Yoda, Y.; Kikuta, S.; Seto, M.; Kimball, C. W.; Dabrowski, B. *Phys. Rev. Lett.* **1995**, *74*, 3832−3835.
(44) Sturhahn, W. *J. Phys.: Condens. Matter* **2004**, *16*, S497−S530.
(45) (a) Zeng, W.; Silvernail, N. J.; Scheidt, W. R.; Sage, J. T. Nuclear Resonance Vibrational Spectroscopy (NRVS). In *Encyclopedia of Inorganic Chemistry*; 2008 (published online). (b) Sage, J. T.; Paxson, C.; Wyllie, G. R. A.; Sturhahn, W.; Durbin, S. M.; Champion, P. M.; Alp, E. E.; Scheidt, W. R. *J. Phys.: Condens. Matter* **2001**, *13*, 7707−7722. (c) Scheidt, W. R.; Barabanschikov, A.; Pavlik, J. W.; Silvernail, N. J.; Sage, J. T. *Inorg. Chem.* **2010**, *49*, 6240−6252.
(46) (a) Xiao, Y.; Wang, H.; George, S. J.; Smith, M. C.; Adams, M. W.; Jenney, F. E., Jr.; Sturhahn, W.; Alp, E. E.; Zhao, J.; Yoda, Y.; Dey, A.; Solomon, E. I.; Cramer, S. P. *J. Am. Chem. Soc.* **2005**, *127*, 14596−14606. (b) Petrenko, T.; George, S. D.; Aliaga-Alcalde, N.; Bill, E.; Mienert, B.; Xiao, Y.; Guo, Y.; Sturhahn, W.; Cramer, S. P.; Wieghardt, K.; Neese, F. *J. Am. Chem. Soc.* **2007**, *129*, 11053−11060. (c) Bell, C. B., III; Wong, S. D.; Xiao, Y.; Klinker, E. J.; Tenderholt, A. L.; Smith, M. C.; Rohde, J. U.; Que, L., Jr.; Cramer, S. P.; Solomon, E. I. *Angew. Chem., Int. Ed.* **2008**, *47*, 9071−9074. (d) Paulat, F.; Berto, T. C.; George, S. D.; Goodrich, L.; Praneeth, V. K.; Sulok, C. D.; Lehnert, N. *Inorg. Chem.* **2008**, *47*, 11449−11451.
(47) Liu, J.-G.; Ohta, T.; Yamaguchi, S.; Ogura, T; Sakamoto, S.; Maeda, Y.; Naruta, Y. *Angew. Chem., Int. Ed.* **2009**, *48*, 9262−9267.
(48) Wertz, D. L.; Valentine, J. S. *Struct. Bonding (Berlin)* **2000**, *97*, 37−60.
(49) Mikhaltseva, I. S.; Gridnev, A. A. *Bull. Acad. Sci. USSR. Div. Chem. Sci.* **1992**, *41*, 1511−1512.
(50) Vogel, K. M.; Kozlowski, P. M.; Zgierski, M. Z.; Spiro, T. G. *J. Am. Chem. Soc.* **1999**, *121*, 9915−9921.
(51) (a) Yoda, Y.; Yabashi, M.; Izumi, K.; Zhang, X. W.; Kishimoto, S.; Kitao, S.; Seto, M.; Mitsui, T.; Harami, T.; Imai, Y.; Kikuta, S. *Nucl. Instrum. Methods Phys. Res., Sect. A* **2001**, *467*, 715−718. (b) Yoda, Y.; Zhang, X.; Kikuta, S. *AIP Conf. Proc.* **2007**, *879*, 926−929.
(52) Kohn, V. G.; Chumakov, A. I.; Rüffer, R. *Phys. Rev. B* **1998**, *58*, 8437−8444.
(53) Frisch, M. J.; Trucks, G. W.; Schlegel, H. B.; Scuseria, G. E.; Robb, M. A.; Cheeseman, J. R.; Montgomery, Jr., J. A.; Vreven, T.; Kudin, K. N.; Burant, J. C.; et al. *Gaussian 03*; Gaussian, Inc.: Wallingford, CT, 2004.
(54) Becke, A. D. *Phys. Rev. A* **1988**, *38*, 3098−3100.
(55) Becke, A. D. *J. Chem. Phys.* **1993**, *98*, 5648−5652.
(56) Lee, C.; Yang, W.; Parr, R. G. *Phys. Rev. B* **1988**, *37*, 785−789.
(57) Krishnan, R.; Binkley, J. S.; Seeger, R.; Pople, J. A. *J. Chem. Phys.* **1980**, *72*, 650−654.
(58) Clark, T.; Chandrasekhar, J.; Spitznagel, G. W.; Schleyer, P. V. *J. Comput. Chem.* **1983**, *4*, 294−301.
(59) Frish, M. J.; Pople, J. A.; Binkley, J. S. *J. Chem. Phys.* **1984**, *80*, 3265−3269.
(60) Leu, B. M.; Zgierski, M. Z.; Wyllie, G. R. A.; Scheidt, W. R.; Sturhahn, W.; Alp, E. E.; Durbin, S. M.; Sage, J. T. *J. Am. Chem. Soc.* **2004**, *126*, 4211−4227.
(61) The script of Gennrvs written by Adam Tenderholt can be found at http://www.stanford.edu/group/solomon/software/gennrvs.py.txt.
(62) Silvernail, N. J.; Roth, A.; Schulz, C. E.; Noll, B. C.; Scheidt, W. R. *J. Am. Chem. Soc.* **2005**, *127*, 14422−14433.
(63) Silvernail, N. J.; Noll, B. C.; Schulz, C. E.; Scheidt, W. R. *Inorg. Chem.* **2006**, *45*, 7050−7052.
(64) 5c CO−heme complexes were reported to coordinate one more CO to yield bis(CO) bound 6c heme complexes: 5c CO−heme adducts and 6c bis(CO) bound heme are in equilibrium with reported ranges of association constants for the first and second CO are (3−7) × 10^4 and 20−330 M^{-1}, respectively. These properties are dependent on porphyrin derivatives, and the data for [Fe(TMP)(CO)] remains to be reported. Scheidt and co-workers successfully crystalized both mono- and bis(CO) bound heme complexes from the same solution in which [Fe^{II}(OEP)] and CO are dissolved.[63] Thus, bis(CO)-bound porphyrin complex could be included in our spectroscopic sample, which might be reflected in uncharacterized small peaks observed in the middle range of NRVS spectrum shown in Figure 2. Thus, the bis(CO) heme complex of [Fe(TMP)$(CO)_2$] was analyzed by DFT calculation, and the NRVS spectrum was simulated, which are shown in Figures S1 and S2 in the Supporting Information, respectively. The NRVS simulation indicates a small amount of bis(CO) complex may be included in the spectroscopic sample.
(65) A relatively large discrepancy between the DFT-predicted vibrational energy of the NRVS prominent peak and the experimental one was observed. Occasionally, relatively large deviations between DFT and observed frequencies (20−50 cm^{-1}) were observed in 5c diatomic bound hemes.[15,50,66] Thus, this discrepancy might arise from a difficulty of DFT to describe the geometric and electronic properties of the 5c CO−heme complex.
(66) Pavilik, J. W.; Barabanschikov, A.; Oliver, A. G.; Alp, E. E.; Sturhahan, W.; Zhao, J.; Sage, J. T.; Scheidt, W. R. *Angew. Chem., Int. Ed.* **2010**, *49*, 4400−4404.
(67) This mode is coupled with peripheral phenyl ring distortion in an out-of-phase manner, and another mode coupled with the

substituent vibration in an in-phase manner was calculated at 565 cm^{-1}.

(68) Klug, D. D.; Zgierski, M. Z.; Tse, J. S.; Liu, Z.; Kincaid., J. R.; Czarnecki, K.; Hemley, R. J. *Proc. Natl. Acad. Sci. U.S.A.* **2002**, *99*, 12526−12530.

(69) In fact, more than one vibrational mode associated with motions in the Fe−Im bond were observed at 191, 194, 208, and 214 cm^{-1}. Multiple contributions of Fe−Im vibrations in the 150−200 cm^{-1} region were previously reported.[12b] However, in our model those modes are significantly coupled with dominant twisting motions of imidazole tethering linker moiety. Thus, we did not assign these modes as the representative Fe−Im vibrations.

(70) This mode is coupled with $(Me)_3$−Ph twisting motion in an out-of-phase manner, and another mode coupled with the substituent vibration in an in-phase manner was calculated at 485 cm^{-1}.

(71) (a) Bersuker, I. B.; Stavrov, S. S. *Coord. Chem. Rev.* **1988**, *88*, 1−68. (b) Bersuka, I. B. *Electronic Structure and Properties of Transition Metal Compounds*; Wiley-Interscience: New York, 1996.

(72) (a) Karlin, K. D. *Nature* **2010**, *463*, 168−169. (b) de Visser, S. P.; Valentine, J. S.; Nam, W. *Angew. Chem., Int. Ed.* **2010**, *49*, 2099−2101.